

The mechanism of acetyl-CoA synthase through the lens of a nickel model system

Received: 15 November 2024

Shounak Nath , Leonel Griego & Liviu M. Mirica

Accepted: 14 May 2025

Published online: 04 June 2025

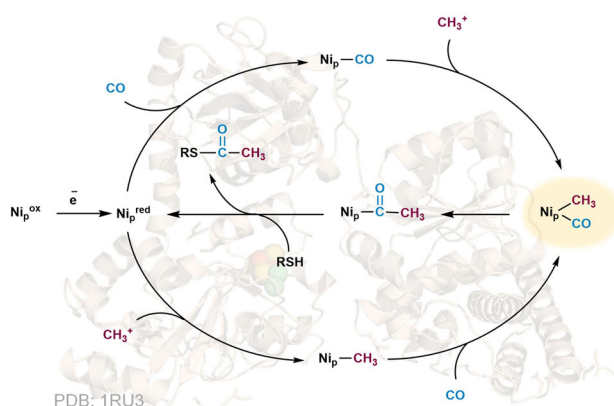
Check for updates

Given the urgent need to develop new methods of CO₂/CO utilization, understanding the mechanism of acetyl-CoA synthase (ACS)—a primordial nickel-containing enzyme that converts these gases into a source of cellular energy—is crucial; however, conflicting hypotheses and a dearth of well-characterized bioorganometallic intermediates have hindered a proper understanding of its mechanism. Herein, we report a functional model system that supports several organometallic intermediates proposed for ACS, including the long sought-after Ni(methyl)(CO) species, and promotes all key reaction steps during catalysis: methylation, carbonylation, and thiolysis. Our investigations provide the following key mechanistic insights that are directly relevant to ACS: (i) the binding of a second CO molecule to the Ni center promotes migratory insertion, (ii) both paramagnetic and diamagnetic Ni intermediates are involved, (iii) one-electron oxidation of the Ni^{II}(acetyl) (thiolate) species drives a fast reductive elimination, and (iv) a random binding order of the methyl and CO groups to the Ni center is feasible.

The microbial nickel-containing enzyme acetyl-CoA synthase (ACS) constitutes a pivotal component of the Wood-Ljungdahl Pathway (WLP), and together with carbon monoxide dehydrogenase (CODH) fixes atmospheric CO₂/CO into the global carbon cycle^{1–5}. In the present context of the ever-increasing imbalance of these gases in the atmosphere, an in-depth understanding of this enzyme pathway is essential to devise new strategies for CO₂/CO fixation into synthetically useful chemicals⁶. Specifically, the mechanism of ACS has parallels to the industrial Monsanto and Cativa processes for acetic acid synthesis, albeit they operate under harsh conditions and employ precious Rh and Ir catalysts^{7,8}. ACS catalyzes the synthesis of acetyl-CoA in the final step of the WLP through the condensation of CO (supplied from CODH via a gas channel), a methyl group (transferred from the methylcobalamin of a corrinoid iron-sulfur protein), and coenzyme A via several organometallic Ni intermediates (Fig. 1a)⁹. In certain microbes, the WLP can operate in the reverse direction, wherein acetyl-CoA is metabolized into CO₂ and methane. The first step in this process is carried out by a related Ni enzyme acetyl-CoA decarbonylase/synthase (ACDS) that reversibly cleaves the acetate C–C bond via a Ni-based decarbonylation reaction^{10,11}. The A cluster in the active site of ACS consists of a dinuclear Ni cluster bridged by two μ₂-thiolates: one of the Ni centres (the distal Ni_d) has a square planar geometry, while the other

Ni centre (the proximal Ni_p) adopts an unusual 3-coordinate geometry and is bridged to a [Fe₄S₄]^{nt} cluster via another μ₂-thiolate (Fig. 1d)¹². It is commonly accepted that the 3-coordinate Ni_p center is the site of substrate binding in the A cluster. Nevertheless, conflicting hypotheses and a dearth of well-characterized bioorganometallic intermediates have hindered a proper understanding of the mechanism of ACS. A Ni(methyl)(CO) intermediate, which has both the methyl and CO groups directly bound to the Ni center, has been proposed to be involved in the enzyme mechanism¹³, yet it has never been observed⁹. This conundrum is exacerbated by the fact that no such intermediate has been isolated in any synthetic model of ACS^{14–17}. Due to the presence of a CO alcove near the active site, and with the recent discovery of a two-CO bound state at the Ni_p center^{18,19}, the role of excess CO on the mechanism of ACS is also not well understood. Although it is known that the enzyme needs a reductive activation from its inactive Ni^{II} state to enter the catalytic cycle²⁰, the precise oxidation states of the catalytically relevant intermediates are ambiguous^{1,5,21}. Finally, the order of binding of the methyl and CO groups to the Ni center, whether ordered or random, has also been debated (Fig. 1a)²².

Synthetic models that mimic the structure and/or the function of ACS are useful to establish molecular principles governing its mechanism. Several organometallic Ni complexes have been

a The proposed mechanism of acetyl-CoA synthase (ACS)**Remaining questions on the mechanism of ACS**

- Uncharacterized intermediate: the Ni(CH₃)(CO) species
- Paramagnetic or diamagnetic Ni intermediates
- Order of binding of CH₃ and CO to the Ni center
- Relevance of a 2nd CO molecule binding to the Ni_p center

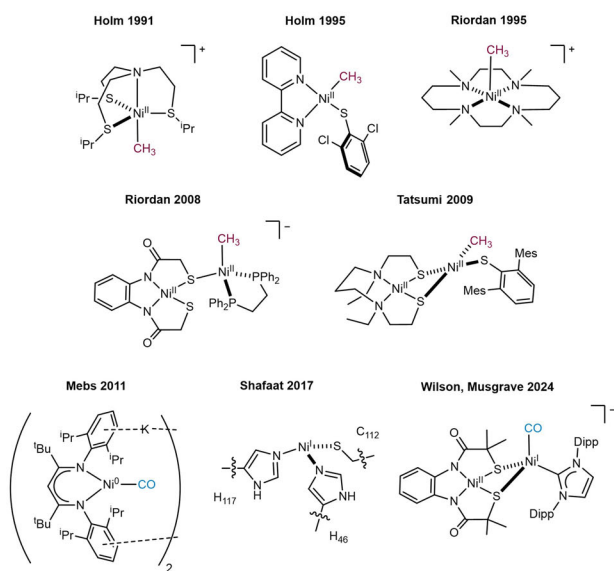
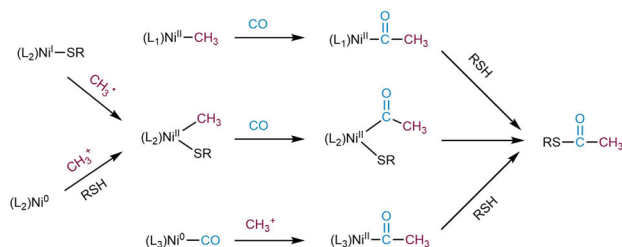
b Reported synthetic models of ACS

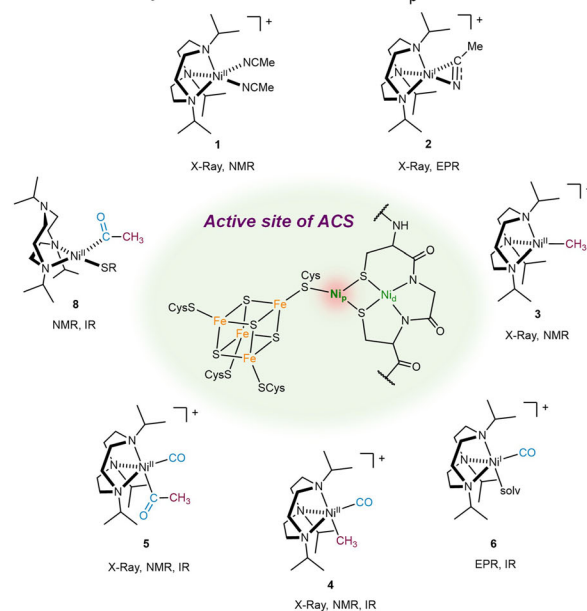
Fig. 1 | Acetyl-CoA Synthase and models. **a** The proposed mechanism for acetyl-CoA synthase (ACS) showing substrate binding at the proximal Ni_p site. Ni intermediates involved can either be paramagnetic (Ni^{II}/Ni^{III}) or diamagnetic (Ni⁰/Ni^I). The two possible substrate binding routes are shown: CO binding followed by methyl (top pathway) and methyl binding followed by CO (bottom pathway)¹. The

developed over the years as models for ACS (Fig. 1b), however, they only showcase a limited set of the proposed enzymatic catalytic steps (Fig. 1c)^{14–16,23–29}. Recently, Shafaat and coworkers have reported a modified azurin protein containing a mononuclear 3-coordinate Ni center as a model for ACS that provided insights into the nature of several proposed organometallic intermediates^{17,30–32}.

Herein, we report a comprehensive study of a synthetic functional mimic of ACS that enables the exploration of most of the organometallic intermediates proposed for the catalytic steps involved in the

c Reported routes to access thioesters with synthetic models

No synthetic ACS model showcases the full set of routes proposed for the enzyme

d This work: synthetic models for the Ni_p center in ACS**Highlights**

- Isolation and reactivity of the Ni^{II}(CH₃)(CO) intermediate
- Both paramagnetic & diamagnetic Ni species observed in the key reaction steps
- Evidence for random order binding of CO & CH₃ to the Ni center
- Binding of a 2nd CO molecule promotes migratory insertion
- 1800-fold enhancement in rate of thioester formation upon one-electron oxidation of Ni^{II}(acetyl)(thiolate) species

crystal structure of the monomeric form of ACS obtained from *Carboxydotherrmus Hydrogenoformans* (PDB: 1RU3) is shown in the background. **b** Reported functional models of ACS that promote formation of thioesters. **c** Synthetic routes to access thioesters with the reported synthetic functional models of ACS. **d** Present work: mononuclear functional models for the Ni_p site of ACS.

ACS mechanism. A series of Ni complexes supported by the tridentate macrocyclic ligand 1,4,7-triisopropyl-1,4,7-triazacyclononane (Pr₃tacn) have been synthesized and their organometallic reactivity was investigated in detail (Fig. 1d), including a very rare Ni^{II}(methyl)(CO) intermediate. In addition, our investigations provide key mechanistic insights that are directly relevant to mechanism of ACS (Fig. S1): (i) the importance of a second CO molecule binding to the Ni centre to drive the CO migratory insertion step, (ii) the relevance of both diamagnetic and paramagnetic Ni intermediates during the catalytic steps, and (iii)

the feasibility of a random binding order of the methyl and CO groups to the Ni center. Finally, we show that (iv) the reductive elimination of the thioester product from the Ni^{II}(acetyl)(thiolate) species is ~1800 times faster upon one-electron oxidation, thus likely proceeding via a Ni^{III} intermediate. Importantly, the mechanistic studies described herein could be adapted to probe the mechanistic details of the ACS/ACDS enzymes.

Results and discussion

A synthetic model for the methylated state of ACS

While ¹Pr₃tacn does not model the sulphur-rich coordination environment of the Ni_p site in the A cluster, it does provide a three-coordinate geometry akin to that of the enzyme. Moreover, the bridging μ₂-thiolates binding to the Ni_p site are weaker in terms of electron donating properties than a classical thiolate, an aspect which the stronger σ-donating N-based ¹Pr₃tacn attempts to mimic. The solvent-bound oxidized Ni^{II} state of ACS (known as A_{ox}) is known to be inactive and needs a reductive activation to a reduced state (known as A_{red}) to enter the catalytic cycle²⁰. Accordingly, the previously reported bis-solvento Ni complex [(¹Pr₃tacn)Ni^{II}(NCMe)₂](PF₆)₂ (**1**) was chosen to model the A_{ox} state of ACS³³. Its Ni^{II}/Ni^I redox couple (−1.20 V vs Fc^{+/0}, −0.56 V vs NHE) compares well to the experimentally estimated redox potential for the Ni^{II} (A_{ox})/Ni^I-CO (A_{NiFeC}) couple of ACS (−0.50 to −0.54 V vs NHE)³⁴ or the computed value for the Ni^{II} (A_{ox})/Ni^I (A_{red}) couple (−0.67 V vs NHE)³⁵, as well as to that of the Ni^{II}/Ni^I redox couple for the Ni-substituted azurin model of ACS³⁰. These comparable redox potentials support a similarity between the model complex **1** and the biological system, especially as related to the reduction of the A_{ox} state of ACS. Accordingly, the one-electron reduction of **1** by cobaltocene (CoCp₂) or K₈ generates the Ni^I complex [(¹Pr₃tacn)Ni^I(η²-NCMe)]PF₆ (**2**), which thus is viewed as a model of the catalytically active reduced state A_{red} of ACS, although there are inherent differences in the nature of reductants employed in the synthetic model and the biological system³⁶.

As a model for the methylated state (A_{Me}) of ACS, the Ni^{II}-monomethyl complex [(¹Pr₃tacn)Ni^{II}(CH₃)]PF₆ (**3**) was synthesized as a purple solid in 82% yield via a transmetallation reaction of **1** with a stoichiometric amount of DABAL-Me₃ (Fig. 2a)^{37–39}. An effective magnetic moment of 2.88 μ_B in MeCN was obtained for **1**, which supports a high spin (S = 1) Ni^{II} center. The solid-state structure revealed a distorted tetrahedral coordination environment (τ₄ = 0.64) at the Ni center (Fig. 2c). Notably, tetrahedral high spin organometallic Ni^{II} complexes are difficult to access, particularly because the strong field σ-donor characteristics of the alkyl group favors spin pairing^{24,31,40}. Although the A_{Me} state observed in ACS is low spin⁹, Shafaat and coworkers showed that a Ni-substituted M121A azurin can replicate all the proposed steps of ACS from a high spin tetrahedral Ni^{II} (CH₃) complex¹⁷. Interestingly, **3** could also be generated in 26% yield via a methyl transfer to the Ni^I complex from the methylcobaloxime Co^{III}(dmgBF₂)₂(CH₃)(py) (dmg = dimethylglyoxime, py = pyridine) in the presence of cobaltocene (CoCp₂) as an external reductant. In this case, the methyl radical is presumably transferred from the reduced methylcobaloxime to the Ni^I center in **2** to form the Ni^{II}-monomethyl complex, analogous to previous reports^{27,29,41}. Recent computational studies on the A cluster have also revealed the possibility of a methyl radical transfer from methylcobalamin to the A_{red} (Ni^I) state of ACS⁴². However, other experimental studies on the enzyme have suggested that a cationic methyl transfer is more likely, forming a putative Ni^{III}-CH₃ species^{43,44}. According to the inverted ligand field hypothesis proposed for the Ni-substituted M121A azurin scaffold, the Ni^{III}-CH₃ species needs a reduction to the Ni^{II}-CH₃ state for further reactions³². Since a Ni^{III}-CH₃ species could not be observed for the (¹Pr₃tacn)Ni system, the results described herein suggest that a one-electron reduction is needed for the methyl transfer to occur from a Co^{III}-CH₃ complex and thus

modeling the methyl transfer step by the methylcobalamin to the reduced Ni_p state of ACS^{1,43}.

As a result of its distorted tetrahedral geometry, **3** exhibits an accessible coordination site, and upon exposure to 1 atm CO in CH₂Cl₂ undergoes an immediate color change from purple to orange. The ¹H NMR spectrum of this reaction mixture shows a paramagnetic-to-diamagnetic spectral change that displays a singlet resonance at δ 0.34 ppm, assigned to Ni-CH₃ group, and continued exposure to CO leads to formation of a new singlet resonance at δ 2.65 ppm, assigned to a Ni^{II}-COCH₃ group, that forms with the concomitant decay of the initial Ni^{II}-CH₃ resonance (Figs. S32 and S33). In addition, in situ monitoring by FT-IR reveals an immediate appearance of a peak at ~2000 cm⁻¹ (assigned to the CO stretch of a Ni^{II}-CO species), which persists throughout the reaction and is accompanied by a subsequent growth of a peak at ~1700 cm⁻¹, assigned to the CO stretch of a Ni^{II}-COCH₃ species (Figs. S36 and S37). Overall, these observations are in support of a two-step reaction of **3** with CO: an initial rapid binding of CO to the vacant coordination site, followed by a slow migratory insertion of CO into the Ni^{II}-CH₃ bond to form a Ni^{II}-COCH₃ species (Fig. 2b). Gratifyingly, exposing **3** to 1 atm CO at −78 °C enabled the isolation of a rare complex [(¹Pr₃tacn)Ni^{II}(CH₃)(CO)]PF₆ (**4**) as an orange, diamagnetic solid in 90% yield, and single crystal X-ray diffraction analysis reveals a trigonal bipyramidal geometry at the Ni center (Fig. 2c). The CH₃ group occupies the axial position trans to N(1), while CO occupies the equatorial position, with N(2)-Ni(1)-C(16) and N(3)-Ni(1)-C(16) bond angles of 135.0(2)° and 139.5(2)°, respectively. Interestingly, the Ni-CH₃ bond remains practically unchanged upon binding of CO to the Ni center (1.988(3) Å vs 1.992(6) Å in **3** and **4**, respectively). This Ni(methyl)(CO) complex is a very rare example of an isolated intermediate during the CO migratory insertion into a Ni-methyl complex and models the elusive Ni(methyl)(CO) intermediate in ACS^{45,46}. Finally, overnight exposure of a THF solution of **3** to 1 atm CO at room temperature followed by vapor diffusion of pentane led to the isolation of orange crystals of [(¹Pr₃tacn)Ni^{II}(COCH₃)(CO)]PF₆ (**5**), with the X-ray structure revealing a distorted square pyramidal geometry at the Ni center and confirming the formation of an Ni(acetyl)(CO) species (Fig. 2c). Thus, although the Ni^{II}-monomethyl complex (**3**) has a high spin configuration, it becomes low spin upon binding of the strong field CO ligand, which models the low spin configuration of intermediates observed in ACS⁹.

In ACS, acetyl-CoA formation is known to proceed via a reversible CO binding/migratory insertion at the Ni center, while ACDS is known to reversibly cleave the C-C bond of acetate via formation of acetyl-CoA, followed by a metal-based decarbonylation reaction^{10,11,47}. In this context, crossover/exchange studies were carried out with isotopically labelled complexes, and addition of **3** to a solution of [(¹Pr₃tacn)Ni^{II}(¹³CH₃)(¹³CO)]PF₆ (**4b**) in CD₂Cl₂ under N₂ led to the formation of the mono-labelled species [(¹Pr₃tacn)Ni^{II}(¹²CH₃)(¹³CO)]PF₆ (**4a**) (Figs. 2d and S47), suggesting that the CO molecule can hop from one Ni^{II}-Me complex to another and thus supporting a reversible initial CO binding to **3**. UV-vis titration experiments reveal a large equilibrium constant of ~10⁴ atm⁻¹ for the CO binding to **3** (Figs. S18 and S19). Introduction of ¹³CO to a solution of **5** in CD₂Cl₂ led to ¹³C enrichment at the Ni-bound CO position, but also at the carbonyl carbon of the acetyl group, all three complexes **5a**, **5b**, and **5c** being detected by ¹³C NMR (Figs. 2e and S50). This exchange of the acetyl carbonyl with free CO provides strong evidence that the migratory insertion of CO into the Ni^{II}-CH₃ bond in **4** is also reversible. Additional support for the reversibility of migratory insertion was obtained from ¹H NMR, wherein it was observed that under static vacuum a solution of **5** slowly converts to **4** (Fig. S35).

The CO migratory insertion is a fundamental organometallic transformation and has been suggested in some studies to be the rate determining step of the entire catalytic process in ACS⁴⁷. A recent discovery of a CO alcove near the active site of ACS presumably allows

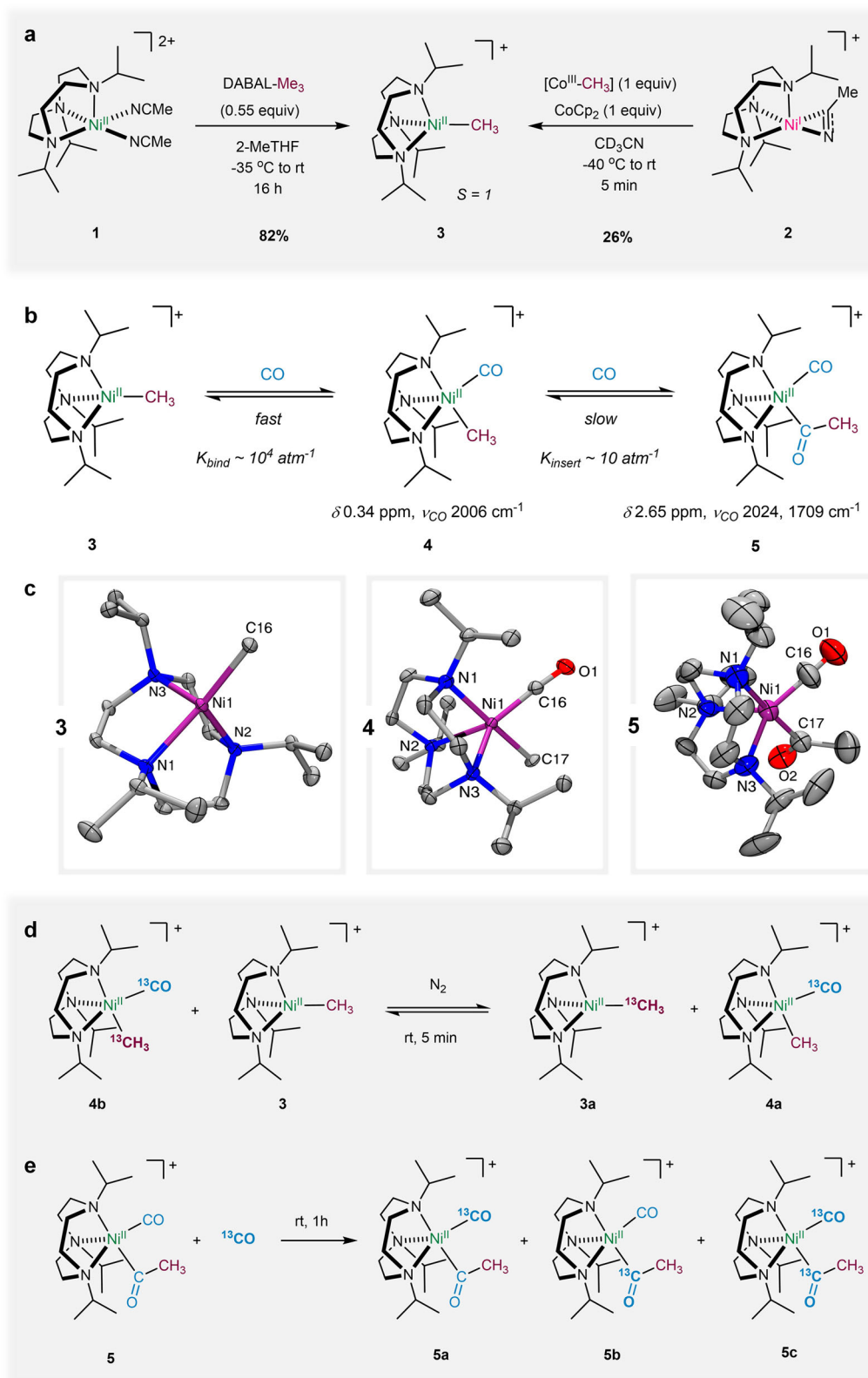


Fig. 2 | Synthesis of models of the methylated state of ACS and its CO reactivity.

a Synthesis of the Ni-monomethyl complex (**3**) as a model for the methylated state of ACS. DABAL-Me₃: bis(trimethylaluminium)-1,4-diazabicyclo[2.2.2]octane; [Co^{III}-CH₃]: Co^{III}(dmgBF₂)₂(CH₃)(py) (dmg dimethylglyoxime, py pyridine); CoCp₂: cobaltocene. **b** The two-step reaction of **3** with CO, to access complexes **4** and **5**. K_{bind} and K_{insert} represent the equilibrium constants for the CO binding and migratory insertion steps, respectively. **c** ORTEP representations with ellipsoids drawn at 50% probability; **3**, selected bond lengths (Å): Ni1-N1, 2.066(3); Ni1-N2,

2.075(3); Ni1-N3, 2.053(3); Ni1-C16, 1.988(3); **4**, selected bond lengths (Å): Ni1-N1, 2.036 (5); Ni1-N2, 2.126(5); Ni1-N3, 2.143(5); Ni1-C16, 1.730(6); Ni1-C17, 1.992(6); C16-O1, 1.140(8); **5**, selected bond lengths (Å): Ni1-N1, 2.092 (5); Ni1-N2, 2.166(5); Ni1-N3, 2.078(5); Ni1-C16, 1.761(9); Ni1-C17, 1.974(7); C16-O1, 1.158(11); C17-O2, 1.201(8). Hydrogen atoms, anions, and non-coordinated solvent molecules were omitted for clarity. **d** ¹³C labelling experiments demonstrating the reversibility of CO binding. **e** ¹³C labelling experiments demonstrating the reversibility of migratory insertion reaction.

for CO saturation conditions during migratory insertion⁴⁸. This is particularly relevant given the recent spectroscopic identification of two CO molecules bound to the Ni_p site¹⁹. In this context, it was observed that **4** undergoes migratory insertion only in the presence of excess CO. Monitoring by UV-vis of the conversion of **4** to **5** under 1 atm CO reveals a first-order growth of an absorption peak at 340 nm, corresponding to the near complete formation (>95%) of the Ni-acetyl complex **5** (Fig. S34), along with a concomitant decay of the absorption peak at 253 nm (Fig. 3a). A rate constant k_{obs} of $1.26 \pm 0.01 \times 10^{-3} \text{ s}^{-1}$ (corresponding to a 2nd order rate constant k_2 of $1.957 \pm 0.01 \times 10^{-1} \text{ M}^{-1} \text{ s}^{-1}$) could be extracted for this process at room temperature by monitoring the peak at 340 nm. Interestingly, k_{obs} was found to increase linearly with an increase in CO concentration (Fig. 3c). This supports a reaction that is first order in CO and indicates an associative binding of CO occurring at or before the rate determining step. An Eyring analysis of this process at various temperatures yields the following activation parameters: $\Delta H^\ddagger = 7 \pm 1 \text{ kcal/mol}$ and $\Delta S^\ddagger = -38 \pm 2 \text{ cal/mol K}$ (Fig. 3d), and a free energy of activation $\Delta G^\ddagger = 18 \pm 1 \text{ kcal/mol}$ (298 K). Importantly, the large negative value for ΔS^\ddagger further supports an associative mechanism for the CO migratory insertion step, as the binding of the second CO molecule leads to a decrease in entropy due to a more ordered transition state.

A solution of **5** is stable only under 1 atm CO and slowly converts to **4** when CO is removed from the headspace of the reaction vessel. The kinetics of this process was followed via UV-vis to reveal a slow first order decay in the peak at 340 nm and a concomitant increase in the peak at 253 nm (Fig. 3b), corresponding to a rate constant for the deinsertion of CO from **5** of $2.03 \pm 0.02 \times 10^{-4} \text{ s}^{-1}$, the CO deinsertion step thus being an order of magnitude slower than the CO migratory insertion. More mechanistic insights were obtained from ¹³C labelling experiments wherein it was observed that the introduction of ¹³CO to a solution of **4** led to the incorporation of CO at all possible sites of the Ni^{II}(COCH₃)(CO) complex (**5a**, **5b**, and **5c**, Fig. S49). This rules out (a) a direct insertion of the incoming CO into the Ni-CH₃ bond and (b) a zero-order process involving an initial CO migratory insertion followed by CO binding, as these two pathways would exclusively lead to the formation of **5b** and **5a**, respectively. Furthermore, the relative fractions of **5a** and **5b** stay nearly equal throughout the reaction (Figs. S51–S53), implying that **5a** and **5b** should arise from a common intermediate. These results are suggestive of an initial binding of CO to the Ni center in **4** to form a transient [LNi^{II}(CH₃)(CO)₂]⁺ species, prior to one of the two CO groups migrating into the Ni-methyl bond (Fig. 3e). This is consistent with the large negative value of ΔS^\ddagger obtained from the Eyring analysis, and also parallels the CO migratory insertion for a phosphine-Ni^{II} complex proposed to operate via a five-coordinate intermediate formed upon coordination of a second CO molecule to the Ni center prior to migratory insertion⁴⁵. Modelling the conversion of **4** to **5** by a two-step reversible process enables the determination of the equilibrium constant for the CO migratory insertion to be $11.9 \pm 5.3 \text{ atm}^{-1}$ (pages S74 and S75), which is three orders of magnitude lower than the equilibrium constant measured for the CO binding to **3** (Fig. 2b). Overall, the equilibrium constant for the conversion of **3** to **5** is determined to be $\sim 10^5 \text{ atm}^{-2}$; by comparison, the equilibrium constant for the CO binding/migratory insertion reaction in ACS is estimated to be 10^4 atm^{-147} .

A synthetic model for the carbonylated Ni^I state of ACS

The Ni^I(CO) intermediate, A_{NiFeC}, is the most well characterized state in ACS^{49,50}, however, there have been questions regarding its involvement in the enzyme catalytic cycle^{51,52}. In an attempt to model this species, exposure of the Ni^I complex **2** to 1 atm CO at -78°C led to an immediate change in the EPR spectrum to yield an axial signal with $g_x = g_y = 2.183$ and $g_z = 2.015$, along with superhyperfine coupling to two N atoms in the g_z direction ($A_{2N} = 14 \text{ G}$, Figs. 3f and S57). Use of ¹³CO instead of ¹²CO led to the appearance of additional coupling in the

g_z direction from the ¹³C ($I = 1/2$) nucleus ($A_C = 14 \text{ G}$), thus confirming the formation of a Ni^I(CO) intermediate. Density functional theory (DFT) calculations reproduce the pseudo-axial g tensor and the superhyperfine coupling constants of the putative [(ⁱPr₃tacn)Ni^I(CO)(NCMe)]⁺ complex **6**, with both CO and MeCN bound to the Ni center (Tables S22 and S23). The spin density plot reveals that the unpaired electron resides mainly on the Ni center (90% of total spin density, and 73% on the d_{z^2} orbital), with small contributions from the N atom of ⁱPr₃tacn, the coordinated CO, and the N atom of the bound acetonitrile (Fig. 3f, inset). Notably, a five-coordinate Ni^I-isocyanide complex supported by the same ligand framework has been reported recently³³, suggesting that such five-coordinate Ni^I complexes with suitable π acceptors can be stabilized with ⁱPr₃tacn. Further confirmation for the formation of a Ni^I(CO) species was obtained from FT-IR, which reveals a CO stretch at 1984 cm^{-1} that red-shifts to 1938 cm^{-1} when ¹³CO is used (Fig. 3g). This shift is consistent with a molecule of CO bound to Ni, as confirmed by DFT calculations (Fig. S104); the extent of CO activation achieved in this model system is comparable to the Ni^I(CO) state in ACS ($\nu_{CO} = 1996 \text{ cm}^{-1}$)⁵³, and also to that in the Ni^I(CO) azurin model of ACS ($\nu_{CO} = 1976 \text{ cm}^{-1}$)³⁰.

Importantly, the Ni^I(CO) species **6** is competent for methylation with the methylcobaloxime Co^{III}(dmgBF₂)₂(CH₃)(py) in presence of CoCp₂ as the reductant, with complex **4** being formed in 46% yield and subsequently leading to formation of **5** upon continued exposure to CO (Fig. 3h). Analogous to the methylation of the Ni^I center in **2**, a methyl radical transfer from the reduced methylcobaloxime to the Ni^I center in **6** is the most likely pathway to form **4**^{16,39}, while the dissociation of the CO ligand from **6** to revert back to the Ni^I precursor **2** prior to methylation seems unlikely (Figs. S63 and S64). Overall, these results suggest the intermediacy of the same Ni^{II}(CH₃)(CO) species **4**, irrespective of the order of addition of CO and CH₃ to the Ni center, and provide strong support for the proposed random binding order of CO and CH₃ to the ACS active site²².

Thiolysis of the synthetic models of ACS

In ACS there is no unambiguous evidence of how CoA binds to the Ni center to promote acetyl-CoA formation^{1,54}. To probe this aspect, complex [(ⁱPr₃tacn)Ni^{II}(CH₃)(SPh)] (**7**) was synthesized from **3**, using thiophenolate as a model for CoA. Upon exposure of **7** to 1 atm CO at -78°C , spectroscopic signatures corresponding to a Ni-bound acetyl group were observed (¹H NMR: δ 2.12 ppm, and IR: ν_{CO} 1628 cm^{-1}), consistent with the formation of the [(ⁱPr₃tacn)Ni^{II}(acetyl)(SPh)] complex (**8**, Fig. 4a)^{23,26,55}. Warming up the above solution to room temperature led to the disappearance of the Ni-acetyl peak and concomitant formation of S-phenyl thioacetate in 77% yield.

Since CoA is proposed to be the final substrate in the catalytic cycle of ACS²², a more faithful synthetic route was employed in which **4** was reacted with PhSNa in THF-*d*₈ at -78°C in the absence of excess CO (Fig. 4b, top), leading to the formation of the same species **8**, as shown by ¹H NMR and FT-IR, and eventual formation of S-phenyl thioacetate in 48% yield (determined by ¹H NMR) at room temperature; this reactivity suggests thiolates behave in a manner similar to CO by driving the CO migratory insertion step. Moreover, the yield of the thioacetate product increases to 77% in the presence of 1 atm CO (Fig. 4b, condition b), and this trend is conserved across a range of aryl and alkyl thiolates with varying electronic and steric preferences (Fig. 4b). Interestingly, the flexible coordination behavior of ⁱPr₃tacn allows it to adopt a κ^2 geometry upon binding of the thiolate to the Ni^{II} center in **4**, and computational studies on the A cluster of ACS suggested a similar de-coordination of one of the μ_2 -thiolates upon the binding of CoA to the Ni_p site⁵⁴. Finally, thiolysis of complex **5** with either aryl or alkyl thiolates also leads to the formation of thioesters in high yields (Fig. 4b, condition c).

Excitingly, a sequential synthetic strategy was employed, starting with the Ni^{II} precursor **1** that is activated via reduction to the Ni^I species

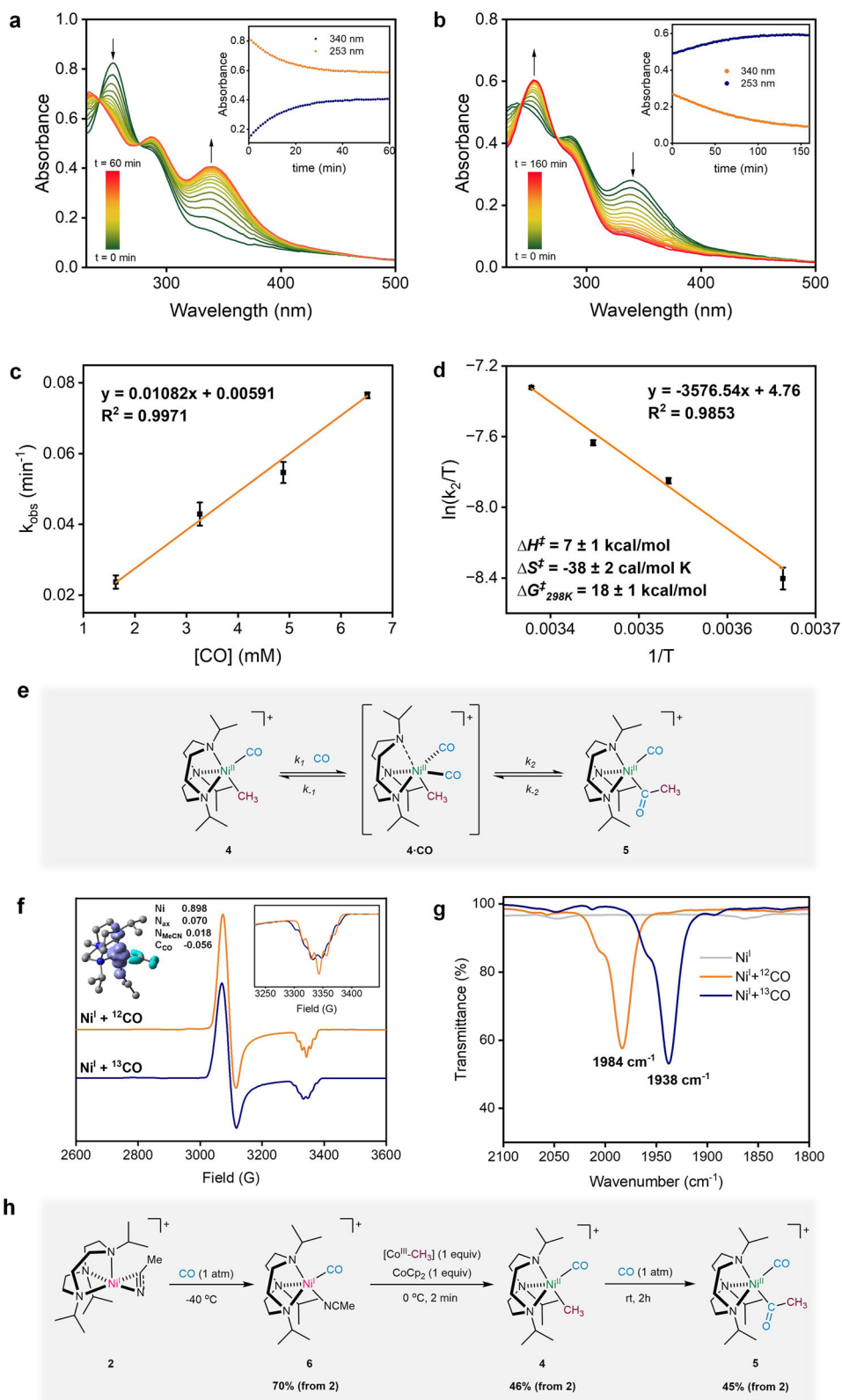


Fig. 3 | CO migratory insertion and the $Ni^I(CO)$ complex supported by Pr_3tactn .

a UV-vis profiles for the reaction of **4** with 1 atm CO to form **5**. **b** UV-vis profiles for the conversion of **5** to **4** under 1 atm N_2 . **c** $[CO]$ dependence on k_{obs} for the CO migratory insertion step; first-order dependence on $[CO]$ is observed. The error bars represent standard error and have been obtained from an average of three independent trials. **d** Eyring plot for the CO migratory insertion for the evaluation of activation parameters. The error bars represent standard error and have been obtained from an average of three independent trials. **e** Proposed mechanism for the CO migratory insertion. **f** Spectroscopic characterization of the (Pr_3tactn)

$Ni^I(CO)$ complex by X-band EPR; spectra collected upon exposure of **2** to 1 atm ^{12}CO or ^{13}CO at $-78^\circ C$, recorded at 77 K in 3:1 PrCN/MeCN. Inset shows the spin density plot drawn at a 0.0025 isovalue. **g** Spectroscopic characterization of the $Ni^I(CO)$ complex supported by Pr_3tactn by solution IR; spectra collected upon exposure of **2** to 1 atm ^{12}CO or ^{13}CO in a solution of MeCN/PrCN (1:3). **h** Methylation of the in situ generated $[(Pr_3tactn)Ni^I(CO)(NCMe)]^+$ complex **6** with the methylcobaloxime in the presence of an external reductant; $[Co^{III}CH_3]$; $Co^{III}(dmgBF_2)_2(CH_3)(py)$ (dmg dimethylglyoxime, py pyridine); $CoCp_2$: cobaltocene.

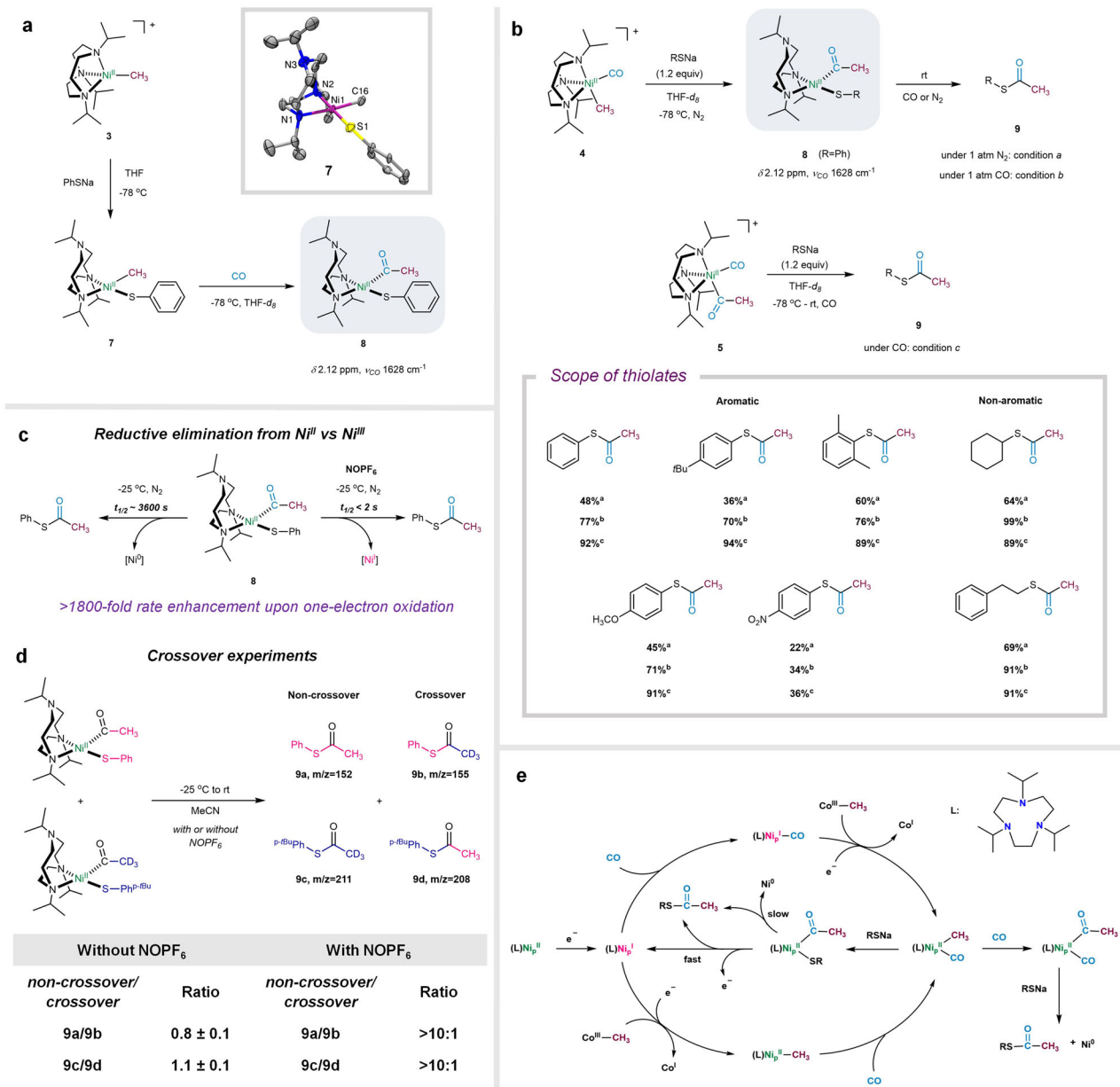


Fig. 4 | Thiolysis of the model Ni complexes. **a** Synthesis of [(Pr₃tacn)Ni^{II}(CH₃)(SPh)] (**7**) and its reaction with CO to form [(Pr₃tacn)Ni^{II}(COCH₃)(SPh)] (**8**); ORTEP representation of **7** shown with ellipsoids drawn at 50% probability. **b** Generation of thioesters via the carbonylated complexes **4** and **5** under three different conditions; condition a: reaction of **4** with thiolates under 1 atm N₂; condition b: reaction of **4** with thiolates under 1 atm CO; condition c: reaction of **5** with thiolates under 1 atm CO. Yields of thioesters obtained from the corresponding aryl/alkyl

thiolates under the three conditions are shown. **c** One-electron oxidation of **8** by NOPF₆ leads to a > 1800-fold rate enhancement for the reductive elimination step. **d** Crossover experiments between [(Pr₃tacn)Ni^{II}(COCD₃)(SPh)] and [(Pr₃tacn)Ni^{II}(COCH₃)(SPh^{t-Bu})] complexes suggest a concerted reductive elimination upon one-electron oxidation. **e** Summary of reactivity pathways for the (Pr₃tacn)Ni^I system described herein, which replicates all key steps in the proposed catalytic cycle of ACS.

2, followed by methylation with Co^{III}(dmgBF₂)₂(CH₃)(py) in presence of a reductant (CoCp₂), carbonylation under 1 atm CO, and thiolysis with thiophenolate led to the formation of S-phenyl thioacetate in 61% yield (Table S4), while switching the order of addition of CO and methyl groups also led to the formation of the product in 34% yield (Table S5). The above example of thioester formation via reductive activation of a Ni^{II} center and independent addition of methyl, CO, and thiolate groups reproduces all key steps of the proposed catalytic cycle for ACS. Importantly, one-electron oxidation of the in situ generated **8** by NOPF₆ leads to a > 1800-fold increase in the rate of thioester formation at -25 °C (Fig. 4c). Additionally, a negligible amount of crossover products are formed when a 1:1 mixture of [(Pr₃tacn)Ni^{II}(COCD₃)(SPh)]

and [(Pr₃tacn)Ni^{II}(COCH₃)(SPh^{t-Bu})] are oxidized with NOPF₆ under an inert atmosphere (Fig. 4d), strongly suggesting that one-electron oxidation drives a rapid, concerted reductive elimination reaction from a transient Ni^{III} intermediate (Fig. S83). The Ni^I species generated during this process is likely trapped by the NO product from NOPF₆ reduction, to form the previously reported [(Pr₃tacn)Ni^I(NO)]⁺ species (Fig. S83)³³; this one-electron oxidation during the thiolysis step can thus be a plausible pathway to regenerate the active catalyst as a Ni^I species, and thus close the reaction cycle and avoid the formation of dead-end Ni⁰ species. Importantly, in ACS a ferredoxin is proposed to act as an electron shuttle that promotes electron transfer steps at both the activation and methylation steps, as well as at the thiolysis step to

form the thioester product and regenerate the active Ni^I species⁵⁶. Thus, based on these model studies we propose Nature may have devised a judicious way to channel an electron to oxidize the Ni^{II}(acetyl)(SCoA) intermediate to a Ni^{III} species that undergoes rapid reductive elimination to regenerate the active Ni^I species (Fig. 4e).

Described herein is a series of (ⁱPr₃tacn)Ni complexes that are functional models of the Ni_p site in ACS and can replicate all key steps in the proposed catalytic cycle of ACS. In addition to isolating the elusive Ni^{II}(methyl)(CO) intermediate, we have demonstrated the chemical competence for both the methyl and CO groups being the first substrate to bind to the Ni^I center and provided insights into the nature of the various organometallic Ni intermediates and the plausible oxidation states of the Ni center during the catalytic mechanism of ACS. Kinetic studies suggest that binding of a second CO molecule to the Ni center can drive the CO migratory insertion step, suggesting that ACS might follow a similar process to promote rapid migratory insertion and the subsequent reductive elimination. The entry point into the catalytic cycle seems to be a Ni^I species that needs suitably timed electron transfers at the methylation and thiolysis steps to form the thioester product, likely via a Ni^{III} species that then regenerates the active Ni^I species in the process. We acknowledge that the mononuclear model described herein does not include the role of the FeS cluster and the Ni_d site in the A cluster of ACS. We envision the Ni_d site is controlling the geometry and tuning the redox potential of the Ni_p site via the bridging μ₂-thiolates, while the FeS cluster might act as a temporary electron storage site that, in conjunction with ferredoxin, aids in the electron shuttling events that we propose to be essential for the the reduction, methylation, and the thiolysis steps needed to complete a catalytic cycle. Overall, we hope that the mechanistic insights obtained from these studies will enable the exploration of the various proposed enzymatic mechanisms, and that the experiments described herein will inspire new enzyme mechanistic studies to gain a better understanding of the function of ACS and ACDS.

Methods

Synthesis of [(ⁱPr₃tacn)Ni^{II}(CH₃)₂](PF₆)₂ (3)

In a N₂ filled glovebox maintained at <1 ppm O₂ levels, a 20 mL vial equipped with a magnetic stir bar was charged with [(ⁱPr₃tacn)Ni^{II}(NCMe)₂](PF₆)₂ (200 mg, 1 equiv, 0.291 mmol) and 5 mL 2-MeTHF. A second 20 mL vial was charged with the bis(trimethylaluminum)-1,4-diazabicyclo[2.2.2]octane adduct, DABAL-Me₃ (41.1 mg, 0.55 equiv, 0.160 mmol) and dissolved in 5 mL 2-MeTHF. Both solutions were cooled to -35 °C and the solution of DABAL-Me₃ was added dropwise to the suspension of [(ⁱPr₃tacn)Ni^{II}(NCMe)₂](PF₆)₂ in 2-MeTHF. The reaction mixture was allowed to warm to room temperature and stirred overnight. The reaction mixture was then filtered to separate a purple precipitate, which was extracted several times with THF to yield a purple solution. The extraction was performed to remove a grey solid that is presumably a byproduct derived from the aluminium reagent. This resulting purple solution was concentrated under vacuum and precipitated by the addition of excess pentane to yield a purple solid (114 mg, 82% yield). Crystals suitable for X-ray diffraction were obtained on cooling a saturated solution of **3** in 2-MeTHF (~5 mg of complex dissolved in 4 mL of solvent) at -35 °C. ¹H NMR (CD₃CN, 500 MHz) δ (ppm) 10.85 (br), 62.74 (br) 87.14 (br). UV-Vis, MeCN: λ, nm (ε, M⁻¹cm⁻¹): 527 (90), 349 (501), 255 (2602). Evan's method: μ_{eff} = 2.883 μ_B (MeCN). EA: calculated for C₁₆H₃₆F₆N₃NiP: C 40.53% H 7.65% N 8.86%; found: C 40.28% H 7.46% N 8.69%.

Synthesis of [(ⁱPr₃tacn)Ni^{II}(CH₃)(CO)]PF₆ (4)

In a N₂ filled glovebox maintained at <1 ppm O₂ levels, a Schlenk tube was charged with **3** (60 mg, 0.126 mmol) in 4 mL CH₂Cl₂. The tube was taken out of the glovebox and cooled to -78 °C. Excess CO was bubbled into the reaction mixture for 1 min upon which the solution underwent an immediate colour change to orange. At such low

temperatures, the migratory insertion reaction of **4** to **5** is very slow and **4** is the exclusive product obtained under these conditions. The reaction mixture was then subjected to three freeze-pump-thaw cycles to remove any excess CO. The solution was then warmed up to room temperature, concentrated under vacuum and precipitated by the addition of pentane, and an orange solid was isolated (59 mg, 93% yield). Crystals suitable for X-ray diffraction were obtained by vapor diffusion of pentane into a THF solution of **4**. ¹H NMR (CD₂Cl₂, 500 MHz) δ (ppm) 3.20 (sept, 6.5 Hz, 3H), 3.01–2.99 (m, 6H), 2.68–2.66 (m, 6H), 1.44 (d, 6.5 Hz, 18H), 0.34 (s, 3H). ¹³C NMR (CD₂Cl₂, 125 MHz) δ (ppm) 179.76, 59.24, 45.21, 19.22, 4.54. UV-Vis, CH₂Cl₂: λ, nm (ε, M⁻¹cm⁻¹): 450 (424), 286 (4745), 252 (8676). IR (ATR): 2006 cm⁻¹ (Ni-CO). EA: calculated for C₁₇H₃₆F₆N₃NiOP·CH₂Cl₂: C 36.83% H 6.52% N 7.16%; found: C 36.89% H 6.52% N 7.68%.

Synthesis of [(ⁱPr₃tacn)Ni^{II}(COCH₃)(CO)]PF₆ (5)

In a N₂ filled glovebox maintained at <1 ppm O₂ levels, **4** (22 mg, 0.044 mmol) was dissolved in 4 mL THF in a vial. The vial was sealed with a rubber septum, removed from the glovebox, and bubbled with CO for 10 min to ensure CO saturation of the solution. The vial was then allowed to stand under the 1 atm CO overnight at room temperature. Following this, pentane was allowed to diffuse into this solution at -35 °C. Orange crystals (15 mg) of **5** were isolated in 64% yield. **5** is unstable under a nitrogen atmosphere and slowly deinserts CO to form **4**. Hence all NMRs for **5** were recorded under 1 atm CO. ¹H NMR (CD₂Cl₂, 500 MHz) δ (ppm) 3.34 (sept, 6.5 Hz, 3H), 2.96–2.95 (m, 6H), 2.62 (s, 3H), 2.57–2.56 (m, 6H), 1.44 (d, 6.5 Hz, 18H). ¹³C NMR (CD₂Cl₂, 125 MHz) δ (ppm) 221.01, 184.15, 59.44, 45.21, 38.10, 18.36. UV-Vis, CH₂Cl₂: λ, nm (ε, M⁻¹cm⁻¹): 450 (437), 340 (2983), 286 (3862), 232 (5189). IR (ATR): 2024 cm⁻¹ (Ni-CO), 1709 cm⁻¹ (Ni-COMe). EA: calculated for C₁₈H₃₆F₆N₃NiO₂P: C 40.78% H 6.84% N 7.93%; found: C 40.87% H 6.89% N 8.07%.

Data availability

The X-ray crystallographic coordinates for structures reported in this study have been deposited at the Cambridge Crystallographic Data Centre (CCDC), under deposition numbers 2376143 (**3**), 2376142 (**4**), 2376140 (**5**), and 2376141 (**7**). These data can be obtained free of charge from the Cambridge Crystallographic Data Centre via www.ccdc.cam.ac.uk/data_request/cif. All data generated and analyzed are included in the Supplementary Information, including synthetic details, spectroscopic characterization of new compounds, mechanistic studies, computational details, and X-ray crystallographic details. Coordinates of DFT optimized geometries are provided in the Source Data file. Source data are provided with this manuscript. All additional data are available from the corresponding author upon request. Source data are provided with this paper.

References

- Ragsdale, S. W. Biological Carbon Fixation by an Organometallic Pathway: Evidence Supporting the Paramagnetic Mechanism of the Nickel-Iron-Sulfur Acetyl-CoA Synthase in *Comprehensive Coordination Chemistry III* Vol. 8 (eds Constable, E. C., Parkin, G. & Que Jr, L.) 611–633 (Elsevier, 2021).
- Kung, Y. & Drennan, C. L. One-Carbon Chemistry of Nickel-Containing Carbon Monoxide Dehydrogenase and Acetyl-CoA Synthase in *The Biological Chemistry of Nickel* Vol. 1 (eds Zamble, D., Rowińska-Żyrek, M. & Kozłowski, H.) 121–148 (The Royal Society of Chemistry, 2017).
- Can, M., Armstrong, F. A. & Ragsdale, S. W. Structure, function, and mechanism of the nickel metalloenzymes, CO dehydrogenase, and acetyl-CoA synthase. *Chem. Rev.* **114**, 4149–4174 (2014).
- Ragsdale, S. W. & Pierce, E. Acetogenesis and the Wood-Ljungdahl pathway of CO₂ fixation. *Biochim. Biophys. Acta, Proteins Proteom.* **1784**, 1873–1898 (2008).

- Lindahl, P. A. Acetyl-coenzyme A synthase: the case for a Ni-based mechanism of catalysis. *J. Biol. Inorg. Chem.* **9**, 516–524 (2004).
- Appel, A. M. et al. Frontiers, opportunities, and challenges in biochemical and chemical catalysis of CO₂ fixation. *Chem. Rev.* **113**, 6621–6658 (2013).
- Kalck, P., Le Berre, C. & Serp, P. Recent advances in the methanol carbonylation reaction into acetic acid. *Coord. Chem. Rev.* **402**, 213078 (2020).
- Yoo, C. et al. Nickel-catalyzed ester carbonylation promoted by imidazole-derived carbenes and salts. *Science* **382**, 815–820 (2023).
- Can, M. et al. Characterization of methyl- and acetyl-Ni intermediates in acetyl CoA synthase formed during anaerobic CO₂ and CO fixation. *J. Am. Chem. Soc.* **145**, 13696–13708 (2023).
- Gu, W. W., Gencic, S., Cramer, S. P. & Grahame, D. A. The A-cluster in subunit β of the acetyl-CoA decarbonylase/synthase complex from *Methanosarcina thermophila*: Ni and Fe K-Edge XANES and EXAFS analyses. *J. Am. Chem. Soc.* **125**, 15343–15351 (2003).
- Gencic, S., Duin, E. C. & Grahame, D. A. Tight coupling of partial reactions in the acetyl-CoA decarbonylase/synthase (ACDS) multi-enzyme complex from *Methanosarcina thermophila*: acetyl C-C bond fragmentation at the A cluster promoted by protein conformational changes. *J. Biol. Chem.* **285**, 15450–15463 (2010).
- Darnault, C. et al. Ni-Zn-[Fe-4-S-4] and Ni-Ni-[Fe-4-S-4] clusters in closed and open subunits of acetyl-CoA synthase/carbon monoxide dehydrogenase. *Nat. Struct. Mol. Biol.* **10**, 271–279 (2003).
- Ragsdale, S. W. & Wood, H. G. Acetate biosynthesis by acetogenic Bacteria - Evidence that carbon-monoxide dehydrogenase is the condensing enzyme that catalyzes the final steps of the synthesis. *J. Biol. Chem.* **260**, 3970–3977 (1985).
- Stavropoulos, P., Muettterties, M. C., Carrie, M. & Holm, R. H. Structural and reaction chemistry of nickel-complexes in relation to carbon-monoxide dehydrogenase - a reaction system simulating acetyl-coenzyme-a synthase activity. *J. Am. Chem. Soc.* **113**, 8485–8492 (1991).
- Horn, B., Limberg, C., Herwig, C. & Mebs, S. The conversion of nickel-bound CO into an acetyl thioester: organometallic chemistry relevant to the acetyl coenzyme A synthase active site. *Angew. Chem. Int. Ed.* **50**, 12621–12625 (2011).
- Yoo, C., Oh, S., Kim, J. & Lee, Y. Transmethylation of a four-coordinate nickel(I) monocarbonyl species with methyl iodide. *Chem. Sci.* **5**, 3853–3858 (2014).
- Manesis, A. C., Yerbulekova, A., Shearer, J. & Shafaat, H. S. Thioester synthesis by a designed nickel enzyme models prebiotic energy conversion. *Proc. Natl. Acad. Sci. USA* **119**, e2123022119 (2022).
- Doukov, T. I., Blasiak, L. C., Seravalli, J., Ragsdale, S. W. & Drennan, C. L. Xenon in and at the end of the tunnel of bifunctional carbon monoxide dehydrogenase/acetyl-CoA synthase. *Biochemistry* **47**, 3474–3483 (2008).
- James, C. D., Wiley, S., Ragsdale, S. W. & Hoffman, B. M. ¹³C electron nuclear double resonance spectroscopy shows acetyl-CoA synthase binds two substrate CO in multiple binding modes and reveals the importance of a CO-binding “Alcove”. *J. Am. Chem. Soc.* **142**, 15362–15370 (2020).
- Tan, X. S., Sewell, C., Yang, Q. W. & Lindahl, P. A. Reduction and methyl transfer kinetics of the α subunit from acetyl coenzyme A synthase. *J. Am. Chem. Soc.* **125**, 318–319 (2003).
- Gencic, S., Duin, E. C. & Grahame, D. A. The two-electron reduced A cluster in acetyl-CoA synthase: preparation, characteristics and mechanistic implications. *J. Inorg. Biochem.* **240**, 112098 (2023).
- Seravalli, J. & Ragsdale, S. W. Pulse-chase studies of the synthesis of acetyl-CoA by carbon monoxide dehydrogenase/acetyl-CoA synthase - Evidence for a random mechanism of methyl and carbonyl addition. *J. Biol. Chem.* **283**, 8384–8394 (2008).
- Tucci, G. C. & Holm, R. H. Nickel-mediated formation of thioesters from bound methyl, thiols, and carbon-monoxide - a possible reaction pathway of acetyl-coenzyme a synthase activity in nickel-containing carbon-monoxide dehydrogenases. *J. Am. Chem. Soc.* **117**, 6489–6496 (1995).
- Ram, M. S. & Riordan, C. G. Methyl transfer from a cobalt complex to Ni(Tmc)(+) Yielding Ni(Tmc)Me(+) - a model for methylcobalamin alkylation of Co dehydrogenase. *J. Am. Chem. Soc.* **117**, 2365–2366 (1995).
- Dougherty, W. G., Rangan, K., O’Hagan, M. J., Yap, G. P. A. & Riordan, C. G. Binuclear complexes containing a methylnickel moiety: relevance to organonickel intermediates in acetyl coenzyme A synthase catalysis. *J. Am. Chem. Soc.* **130**, 13510–13511 (2008).
- Ito, M., Kotera, M., Matsumoto, T. & Tatsumi, K. Dinuclear nickel complexes modeling the structure and function of the acetyl CoA synthase active site. *Proc. Natl. Acad. Sci. USA* **106**, 11862–11866 (2009).
- Matsumoto, T., Ito, M., Kotera, M. & Tatsumi, K. A dinuclear nickel complex modeling of the Ni-d(II)-Ni-p(I) state of the active site of acetyl CoA synthase. *Dalton Trans.* **39**, 2995–2997 (2010).
- Wilson, D. W. N. et al. Mixed valence {Ni²⁺Ni¹⁺} clusters as models of acetyl coenzyme A synthase intermediates. *J. Am. Chem. Soc.* **146**, 21034–21043 (2024).
- Ram, M. S. et al. Kinetics and mechanism of alkyl transfer from organocobalt(III) to nickel(I): implications for the synthesis of acetyl coenzyme A by CO dehydrogenase. *J. Am. Chem. Soc.* **119**, 1648–1655 (1997).
- Manesis, A. C., O’Connor, M. J., Schneider, C. R. & Shafaat, H. S. Multielectron chemistry within a model nickel metalloprotein: mechanistic implications for acetyl-CoA synthase. *J. Am. Chem. Soc.* **139**, 10328–10338 (2017).
- Manesis, A. C. et al. A biochemical nickel(I) state supports nucleophilic alkyl addition: a roadmap for methyl reactivity in acetyl coenzyme A synthase. *Inorg. Chem.* **58**, 8969–8982 (2019).
- Kisgeropoulos, E. C., Manesis, A. C. & Shafaat, H. S. Ligand field inversion as a mechanism to gate bioorganometallic reactivity: investigating a biochemical model of acetyl CoA synthase using spectroscopy and computation. *J. Am. Chem. Soc.* **143**, 849–867 (2021).
- Griego, L., Woods, T. J. & Mirica, L. M. A five-coordinate Ni(I) complex supported by 1,4,7-triisopropyl-1,4,7-triazacyclononane. *Chem. Commun.* **58**, 7360–7363 (2022).
- Can, M., Giles, L. J., Ragsdale, S. W. & Sarangi, R. X-ray absorption spectroscopy reveals an organometallic Ni-C bond in the CO-treated form of acetyl-CoA synthase. *Biochemistry* **56**, 1248–1260 (2017).
- Chmielowska, A., Lodowski, P. & Jaworska, M. Redox potentials and protonation of the A-cluster from acetyl-CoA synthase. A density functional theory study. *J. Phys. Chem. A* **117**, 12484–12496 (2013).
- Griego, L., Chae, J. B. & Mirica, L. M. A bulky 1,4,7-triazacyclononane and acetonitrile, a Goldilocks system for probing the role of Ni^{III} and Ni^I centers in cross-coupling catalysis. *Chem* **10**, 867–881 (2024).
- Biswas, K., Prieto, O., Goldsmith, P. J. & Woodward, S. Remarkably stable (MeAl)₂DABCO and stereoselective nickel-catalyzed AIR (R = Me, Et) additions to aldehydes. *Angew. Chem., Int. Ed.* **44**, 2232–2234 (2005).
- Zhang, A. L. et al. Nickel-mediated stepwise transformation of CO to acetaldehyde and ethanol. *Organometallics* **36**, 3135–3141 (2017).
- Somerville, R. J. et al. Ni(I)-alkyl complexes bearing phenanthroline ligands: experimental evidence for CO₂ insertion at Ni(I) centers. *J. Am. Chem. Soc.* **142**, 10936–10941 (2020).
- Abubekkerov, M., Gianetti, T. L., Kunishita, A. & Arnold, J. Synthesis and characterization of coordinatively unsaturated nickel(II) and manganese(II) alkyl complexes supported by the hydrotris(3-

- phenyl-5-methylpyrazolyl)borate (TpPh,Me) ligand. *Dalton Trans.* **42**, 10525–10532 (2013).
41. Demarteau, J., Debuigne, A. & Detrembleur, C. Organocobalt complexes as sources of carbon-centered radicals for organic and polymer chemistries. *Chem. Rev.* **119**, 6906–6955 (2019).
 42. Chen, S. L. & Siegbahn, P. E. M. Insights into the chemical reactivity in acetyl-CoA synthase. *Inorg. Chem.* **59**, 15167–15179 (2020).
 43. Seravalli, J., Brown, K. L. & Ragsdale, S. W. Acetyl coenzyme A synthesis from unnatural methylated corrinoids: requirement for “base-off” coordination at cobalt. *J. Am. Chem. Soc.* **123**, 1786–1787 (2001).
 44. Tan, X. S., Sewell, C. & Lindahl, P. A. Stopped-flow kinetics of methyl group transfer between the corrinoid-iron-sulfur protein and acetyl-coenzyme A synthase form. *J. Am. Chem. Soc.* **124**, 6277–6284 (2002).
 45. Shultz, C. S., DeSimone, J. M. & Brookhart, M. Four- and five-coordinate CO insertion mechanisms in d(8)-nickel(III) complexes. *J. Am. Chem. Soc.* **123**, 9172–9173 (2001).
 46. Shultz, C. S., DeSimone, J. M. & Brookhart, M. Cationic four- and five-coordinate nickel(II) complexes: insights into the nickel(II)-catalyzed copolymerization of ethylene and carbon monoxide. *Organometallics* **20**, 16–18 (2001).
 47. Tan, X. S., Surovtsev, I. V. & Lindahl, P. A. Kinetics of CO insertion and acetyl group transfer steps, and a model of the acetyl-CoA synthase catalytic mechanism. *J. Am. Chem. Soc.* **128**, 12331–12338 (2006).
 48. Wiley, S. et al. An alcove at the acetyl-CoA synthase nickel active site is required for productive substrate CO binding and anaerobic carbon fixation. *J. Biol. Chem.* **300**, 107503 (2024).
 49. Ragsdale, S. W., Wood, H. G. & Antholine, W. E. Evidence that an iron-nickel carbon complex is formed by reaction of Co with the Co dehydrogenase from *Clostridium-thermoaceticum*. *Proc. Natl. Acad. Sci. USA* **82**, 6811–6814 (1985).
 50. Cohen, S. E. et al. Crystallographic characterization of the carbonylated A-cluster in carbon monoxide dehydrogenase/acetyl-CoA synthase. *ACS Catal.* **10**, 9741–9746 (2020).
 51. Seravalli, J., Kumar, M. & Ragsdale, S. W. Rapid kinetic studies of acetyl-CoA synthesis: evidence supporting the catalytic intermediacy of a paramagnetic NiFeC species in the autotrophic Wood-Ljungdahl pathway. *Biochemistry* **41**, 1807–1819 (2002).
 52. Gencic, S., Kelly, K., Ghebreamlak, S., Duin, E. C. & Grahame, D. A. Different modes of carbon monoxide binding to acetyl-CoA synthase and the role of a conserved phenylalanine in the coordination environment of nickel. *Biochemistry* **52**, 1705–1716 (2013).
 53. Kumar, M. & Ragsdale, S. W. Characterization of the Co binding-site of carbon-monoxide dehydrogenase from *Clostridium-thermoaceticum* by infrared-spectroscopy. *J. Am. Chem. Soc.* **114**, 8713–8715 (1992).
 54. Webster, C. E., Darensbourg, M. Y., Lindahl, P. A. & Hall, M. B. Structures and energetics of models for the active site of acetyl-coenzyme a synthase: role of distal and proximal metals in catalysis. *J. Am. Chem. Soc.* **126**, 3410–3411 (2004).
 55. Ariyananda, P. W. G., Kieber-Emmons, M. T., Yap, G. P. A. & Riordan, C. G. Synthetic analogs for evaluating the influence of N-H center dot center dot center dot S hydrogen bonds on the formation of thioester in acetyl coenzyme a synthase. *Dalton Trans.* **38**, 4359–4369 (2009).
 56. Bender, G. & Ragsdale, S. W. Evidence that ferredoxin interfaces with an internal redox shuttle in Acetyl-CoA synthase during reductive activation and catalysis. *Biochemistry* **50**, 276–286 (2011).

Acknowledgements

We thank the National Science Foundation (CHE 2155160 to L.M.M.) for support. We thank all the research facilities in the School of Chemical Sciences at the University of Illinois Urbana-Champaign for their help. We also thank Dr. Toby J. Woods for assistance with the data collection for determining the solid-state structures, and Sagnik Chakrabarti for helpful discussions related to this project.

Author contributions

L.M.M., S.N., and L.G. conceived the overall project. S.N. and L.M.M. conceived and designed the experiments and computations. S.N. and L.G. carried out the experimental work. S.N. analyzed the data. S.N. and L.M.M. wrote the manuscript. L.M.M. directed the project.

Competing interests

The authors declare no competing interests.

Additional information

Supplementary information The online version contains supplementary material available at <https://doi.org/10.1038/s41467-025-60163-z>.

Correspondence and requests for materials should be addressed to Liviu M. Mirica.

Peer review information *Nature Communications* thanks Stephen Ragsdale and the other, anonymous, reviewer(s) for their contribution to the peer review of this work. A peer review file is available.

Reprints and permissions information is available at <http://www.nature.com/reprints>

Publisher’s note Springer Nature remains neutral with regard to jurisdictional claims in published maps and institutional affiliations.

Open Access This article is licensed under a Creative Commons Attribution-NonCommercial-NoDerivatives 4.0 International License, which permits any non-commercial use, sharing, distribution and reproduction in any medium or format, as long as you give appropriate credit to the original author(s) and the source, provide a link to the Creative Commons licence, and indicate if you modified the licensed material. You do not have permission under this licence to share adapted material derived from this article or parts of it. The images or other third party material in this article are included in the article’s Creative Commons licence, unless indicated otherwise in a credit line to the material. If material is not included in the article’s Creative Commons licence and your intended use is not permitted by statutory regulation or exceeds the permitted use, you will need to obtain permission directly from the copyright holder. To view a copy of this licence, visit <http://creativecommons.org/licenses/by-nc-nd/4.0/>.

© The Author(s) 2025